Energy Release Rate of a Mode-I Crack in Pure Shear Specimens Subjected to Large Deformation

Bangguo Zhu¹, Jikun Wang², Alan T. Zehnder¹, Chung-Yuen Hui^{1,3,*}

Abstract

The Pure Shear (PS) crack specimen is widely employed to assess the fracture toughness of soft elastic materials. It serves as a valuable tool for investigating the behavior of crack growth in a steady-state manner following crack initiation. One of its advantages lies in the fact that the energy release rate (J) remains approximately constant for sufficiently long cracks, independent of crack length. Additionally, the PS specimen facilitates the easy evaluation of J for long cracks by means of a tension test conducted on an uncracked sample. However, the lack of a published expression for short cracks currently restricts the usefulness of this specimen. To overcome this limitation, we conducted a series of finite element (FE) simulations utilizing three different constitutive models, namely the neo-Hookean (NH), Arruda-Boyce (AB), and Mooney-Rivlin (MR) models. Our finite element analysis (FEA) encompassed practical crack lengths and strain levels. The results revealed that under a fixed applied displacement, the energy release rate (J) monotonically increases with the crack length for short cracks, reaches a steady-state value when the crack length exceeds the height of the specimen, and subsequently decreases as the crack approaches the end of the specimen. Drawing from these findings, we propose a simple closed-form expression for J that can be applied to most hyper-elastic models and is suitable for all practical crack lengths, particularly short cracks.

Keywords: Finite strain, Hyper-elasticity, Finite element analysis, Edge effect

¹Sibley School of Mechanical and Aerospace Engineering, Field of Theoretical and Applied Mechanics, Cornell University, Ithaca, New York, 14853, USA

²Sibley School of Mechanical and Aerospace Engineering, Cornell University, Ithaca, NY 14853, USA

³Global Station for Soft Matter, GI-CoRE, Hokkaido University, Sapporo 001-0021, Japan

^{*} Corresponding Author, email: ch45@cornell.edu

1. Introduction

The pure shear specimen, proposed by Rivlin and Thomas (Rivlin and Thomas, 1953), is a valuable tool in material research. It enables researchers to measure properties like fracture toughness (Qi et al., 2019; Tanaka et al., 2005; Zheng et al., 2021) and to study crack growth dynamics (Zhang et al., 2022). The initial configuration of the Pure Shear (PS) crack specimen, in its stress-free state, is depicted in Figure 1. The sample has a height of h and a width of w. To be considered as a PS sample, it is required that the *aspect ratio*, w/h, is significantly greater than 1. In addition, the sample thickness must be small compared to h, thereby satisfying the condition for a plane stress state. Theoretically, an idealized PS sample should be an infinite strip (w = infinity in Figure 1) with a semi-infinite crack. However, in practice, such a sample does not exist. In experiments, the crack length, denoted as c, typically exceeds h/2 but considerably less than w. Typical geometries used in experiments are w/h = 5 with c/h = 1 (Pan et al., 2023; Zhang et al., 2022), or w/h = 10/3 with c/h = 2/3 (Zheng et al., 2021). Here we consider the crack length spanning the entire range of the specimen width, i.e., $c \in (0, w)$. In testing, the specimen is clamped to a stiff machine at the upper and lower edges of the specimen, i.e., $Y = \pm h/2$ and a uniform vertical displacement $\pm \Delta/2$ is applied at the clamps.

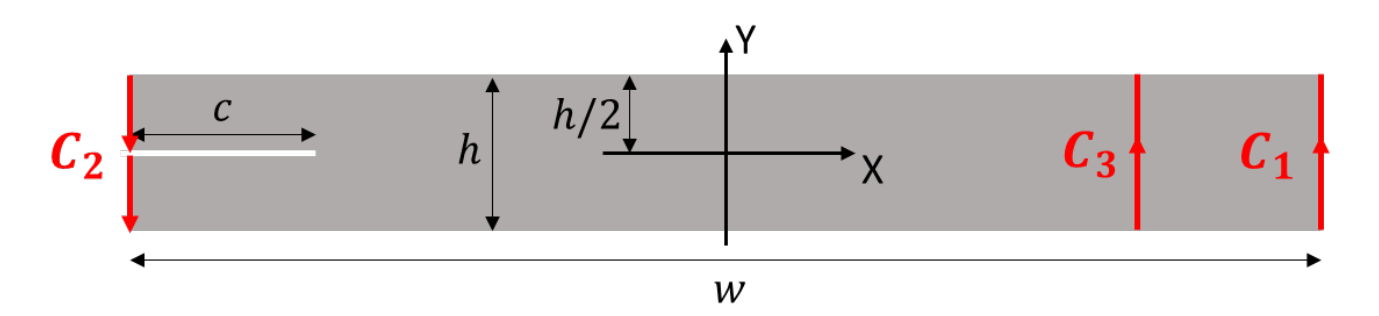


Figure 1: Cross-section geometry of a pure shear (PS) crack sample in its reference unstressed state. The aspect ratio, w/h, should be much greater than 1. The thickness of sample is much smaller than h, so plane stress condition prevails. The direct lines C_1 , C_2 are integration paths for the J integral. On C_3 the deformation state is assumed to be in a state of pure shear. In testing, the upper and lower edges at $Y = \pm h/2$ are clamped to a stiff machine and a vertical displacement of $\pm \Delta/2$ are imposed on these edges.

For elastic solids, this specimen offers several advantages:

- Energy Release Rate: The energy release rate J remains constant across a wide range of crack lengths. This characteristic simplifies the analysis and interpretation of fracture behavior.
- Ease of Computing Energy Release Rate: $J = hW_{\infty}$, where W_{∞} is the strain energy density of an ideal $(w/h \to \infty)$ pure shear uncracked specimen subjected to a vertical stretch. This formula

incorporates all the material behavior into W_{∞} , greatly simplifying the interpretation of this crucial parameter.

• Determination from Tensile Tests: W_{∞} can be determined by conducting a stretching test on an uncracked PS specimen. This method provides a convenient and practical way to obtain J.

The mentioned advantages are contingent upon certain assumptions, some of these were investigated in prior research (Kahle et al., 2023; Pidaparti et al., 1989; Yeoh, 2001). For example, the energy release rate derived by Rivlin and Thomas (Rivlin and Thomas, 1953) did not account for edge effects. Therefore, the actual energy release rate may differ from this value unless the crack is "sufficiently long" and the samples have "large" aspect ratios. The questions are: What criteria define "sufficiently long" or "large"? and how do these criteria depend on the strain hardening characteristics or the applied stretch ratio? For instance, Treloar used an aspect ratio of 15 in his classic experiments (Treloar, 1944), while in recent years, many researchers used considerably smaller aspect ratios. More specifically, Pan et. al., (Pan et al., 2023) and Zhang et al., (Zhang et al., 2022) used an aspect ratio of 5 while Zheng et al., (Zheng et al., 2021) used an aspect ratio of 10/3. Smaller aspect ratio samples are preferred due to the challenges of clamping wide samples made of soft elastic materials. Due to limited availability and the need for homogeneity, small samples are employed in biological material research.

Using stretching data from an uncracked PS sample to determine W_∞ can lead to additional error. Yeoh (Yeoh, 2001) conducted a study using a neo-Hookean model and finite element analysis (FEA). The study revealed that the force required to stretch an uncracked PS sample can be 10% less than that of an ideal, uncracked PS sample $(w/h \to \infty)$, unless the aspect ratio is greater or equal to 5. This result highlights the importance of the end effects and suggested that W_∞ determined using a stretch test can be underestimated by more than 10% for specimens with aspect ratios smaller than 5. In the same paper (Yeoh, 2001), Yeoh also studied the dependence of J on crack length. In a recent study by Kahle et al. (Kahle et al., 2023), the influence of aspect ratio on J was investigated. Their samples had a *fixed* crack length of 20 mm and a width of 60 mm. In their simulations, the aspect ratios were varied by adjusting the sample height. Their findings indicate that, for the given crack length, J is within 10% of its ideal value if the aspect ratio is greater than 2.

Our paper aims to address existing gaps in literature. We carefully carried out a series of finite element simulations using Abaqus. We achieve improved resolution and present a more universally applicable approximation expression upon normalization, in comparison to the work of Pidaparti et al. (Pidaparti et al., 1989), in which virtual crack extension method was used. Also, we investigate the effects of strong

strain stiffening at large stretches by using Arruda-Boyce (AB) constitutive model (Arruda and Boyce, 1993). Effects of weaker hardening are investigated by using the Mooney-Rivlin (MR) model (Mooney, 1940; Rivlin, 1948a). This feature was not considered in Yeoh's work (Yeoh, 2001) which was based on the neo-Hookean model (Rivlin, 1948b). Additionally, we are especially interested in examining the relationship between energy release rate and crack length, a topic that Kahle et al. (Kahle et al., 2023) did not study. As stated by Kahle et al. (Kahle et al., 2023), their findings are influenced by the strain stiffening behavior of the polymer, which makes it difficult to establish a universal criterion. We also study how aspect ratio, stretch and the constitutive model effects the evaluation of W_{∞} . One notable outcome of our current work is the presentation of a simple analytical formula for the energy release rate, which is applicable to most practical crack lengths and stretch ratio.

Our motivation to examine the relation between energy release rate and crack length originates from crack growth experiments. While the works of Yeoh (Yeoh, 2001) and Kahle et al., (Kahle et al., 2023) predominantly concentrate on the determination of fracture toughness, the use of a PS specimen also provides valuable information into crack growth dynamics. Traditionally, a long initial crack is used in crack growth experiments to maintain a constant energy release rate throughout the experiment. However, conducting experiments with short cracks can also yield valuable information. In a recent study conducted by our research group (Wang et al., 2023), we studied delayed fracture in Polydimethylsiloxane (PDMS) using short cracks in PS samples (with aspect ratio w/h=35/10), a departure from the standard long-crack experiments. As we will show, cracks growing from a short starter crack grow into an increasing energy release rate field and thus we attain in a single sample a full range of crack speeds and energy release rates. This enables us to systematically investigate the relationship between crack growth rates and the energy release rate by manipulating the initial crack length.

Another experimental example is the work of (Stoček et al., 2013) where they conducted a fatigue test on a pure-shear specimen with a short initial crack length. Their approach allows them to acquire fatigue crack growth rate over a wide range using a single specimen and cyclic stretch level.

The paper is structured as follows: Section 2 outlines our approach for deriving a formula for the energy release rate that accommodates practical crack lengths and different strain stiffening behavior. In Section 3, we present the finite element analysis (FEA) that assesses the validity of our approach from Section 2. We also present a useful formula which relates the energy release rate to the crack length. Finally, the paper concludes with a discussion and summary.

2. Energy release rate (J) and Material Model

2.1 Energy release rate (J)

In the following, the material behavior is taken to be isotropic, hyper-elastic and incompressible with strain energy density function $W = \Phi(I_1, I_2)$, where $I_1 = trC$, $I_2 = \left[\left(trC\right)^2 - tr\left(C^2\right)\right]/2$ are invariants of the right Cauchy-Green tensor C. As shown by Rice (Rice, 1968) and Knowles and Sternberg (Knowles and Sternberg, 1972), the energy release rate of a crack in an elastic solid can be computed using the path independent integral J. For the PS sample in Figure 1, the finite strain version of J is given by:

$$J = \int_{-h/2}^{h/2} \hat{\Phi}(X = w/2, Y) dY - \int_{-h/2}^{h/2} \hat{\Phi}(X = -w/2, Y) dY,$$
(1)

where $\hat{\Phi}(X,Y) \equiv \Phi\left(I_1(X,Y),I_2(X,Y)\right)$ denotes the strain energy density of a material point located at (X,Y) in the reference configuration. Here, we choose a certain path, although these integrals can be evaluated for any X well ahead of the crack and any X well behind the crack, respectively. The energy release rate of a PS specimen with a long crack is obtained by taking w/h to infinity. In this limit, the stress and strain at distances far behind the crack tip is zero, so $\hat{\Phi}(X=-w/2,Y)=0$ while the stress and strain field far ahead of the crack is homogeneous and is identical to stretching an uncracked, ideal (aspect ratio $w/h \to \infty$) PS specimen uniaxially with stretch ratio $\lambda = \Delta/h$. Specifically, $I_1 = I_2 = \lambda^2 + \lambda^{-2} + 1$ on C_3 , so the strain energy density on C_3 is related to the applied stretch ratio λ by $W_\infty(\lambda) = \Phi(\lambda^2 + \lambda^{-2} + 1, \lambda^2 + \lambda^{-2} + 1)$, independent of position. Thus, in a typical PS sample with a sufficiently long crack, we obtain the result of Rivlin and Thomas (Rivlin and Thomas, 1953):

$$J = \int_{C_1 + C_2} W dY = \int_{-h/2}^{h/2} \hat{\Phi}(X = w/2, Y) dY = \int_{C_3} W_{\infty}(\lambda) dY = hW_{\infty}(\lambda) \equiv J_{\infty}$$
 (2)

Note W_{∞} in Eq. (2) can be obtained experimentally by determining the area under the nominal stress versus stretch ratio curve in a stretch test of an uncracked PS sample, as was done by (Zheng et al., 2021).

Equation (2) is not suitable in two situations: when the crack length is small compared with the height of the specimen or when it is excessively long. In the first scenario, the second integral in Eq. (1) cannot be ignored, even though the first integral in Eq. (1) can still be well approximated by Eq. (2). In the second scenario, the crack is so long that it approaches the right end of the specimen. As a result, the deformation

state along C₃ is no longer homogeneous, so the first integral in Eq. (1) may no longer be accurately represented by Eq. (2). Obviously, for long cracks, the second integral can be safely neglected.

Since J depends solely on the strain energy density evaluated along paths C_1 or C_3 , dimensional analysis implies that

$$J = hW_{\infty} f\left(c/h, w/h, \Delta/H, c_{i}\right)$$
(3)

Here $f(c/h, w/h, \Delta/H, c_i)$ is a dimensionless function and c_i , i = 1, 2, ... are dimensionless parameters in the constitutive model.

Later we will see from the simulation results for the material models, range of stretch ratios and aspect ratios we studied, the dimensionless function f can be well approximated by a simple form. Note for small crack lengths, i.e., $c/h \ll 1$, we can expand f in a Taylor series about c/h = 0. Since J = 0 when c = 0, the first term expansion of the series is:

$$J \approx \alpha W_{\infty} c$$
, $c / h << 1$ (4)

where $\alpha = F\left(w/h, \Delta/H, c_i\right) \equiv df/d\left(c/h\right)\Big|_{c/h=0}$ and is expected to approach a constant for large w/h. Equation (4) is J for short cracks. This result is consistent with a previous analysis of Rivlin (Rivlin and Thomas, 1953) for single edge crack specimens.

2.2 Material models:

We consider incompressible isotropic hyper-elastic solids. Even with these assumptions, the number of constitutive models for nonlinear elasticity is far too many to explore. We focus on energy functions that depend only on I_1 , although the important case of MR which depends on I_1 and I_2 is also considered. The models used in FEA are: (1) neo-Hookean (NH) (Rivlin, 1948b), (2) Arruda-Boyce (AB) (Arruda and Boyce, 1993), and (3) Mooney-Rivlin (MR) (Mooney, 1940; Rivlin, 1948a). Note models (2) and (3) represent two ends of the spectrum of stiffening behavior, i.e., the neo-Hookean model has little provision for strain hardening, whereas the Arruda-Boyce model has finite extensibility. In addition, in uniaxial tension, the MR solid strain softens in comparison relative to the NH solid. Thus, our choice of strain energy density function should cover the full spectrum of strain stiffening behavior. The strain energy density function for the NH and MR models are:

$$W_{NH} = \frac{\mu}{2} [I_1 - 3], \quad W_{MR} = c_1 [I_1 - 3] + c_2 [I_2 - 3]$$
 (5a, b)

where μ is the shear modulus in all three models. In Mooney-Rivlin model, $\mu = 2(c_1 + c_2)$. It is interesting to note that W_{∞} is the same for MR and NH model since $I_1 = I_2$ on C_3 . The AB strain energy density follows the implementation in ABAQUS, which is a truncated form of the original AB model, i.e.:

$$W^{AB} = \mu_0 \left[\frac{\left(I_1 - 3 \right)}{2} + \frac{\left(I_1^2 - 9 \right)}{20n} + \frac{11\left(I_1^3 - 27 \right)}{1050n^2} + \frac{19\left(I_1^4 - 81 \right)}{7000n^3} + \frac{519\left(I_1^5 - 243 \right)}{673750n^4} \right]$$
 (5c)

where n is the number of chain segments. The factor n in AB model represents the limit of chain extensibility where the strain energy goes to infinity. Note that in the truncated form, although the strain hardening behavior can be captured, the strain energy density does not approach infinity as $I_1 \to 3n$. The small strain shear modulus μ , is related to μ_0 in Eq. (5c) by

$$\mu = \mu_0 \left(1 + \frac{3}{5n} + \frac{99}{175n^2} + \frac{513}{875n^3} + \frac{42039}{67375n^4} \right). \tag{5d}$$

 W_{∞} corresponding to these models is obtained by substituting $I_1=I_2=\lambda^2+\lambda^{-2}+1$ into Eq. (5a-c). The key idea is that if Eq. (3) is valid, a plot of $\overline{J}\equiv J/J_{\infty}$ against the normalized crack length $\overline{c}\equiv c/h$ should demonstrate independence from the material model employed. For instance, in the case of the AB model, the plot of \overline{J} should remain the same regardless of the choice of n, while in the MR model, it should be independent of c_1/c_2 . In this study, computations are performed using $\sqrt{n}=3$ and $\sqrt{n}=7$ for the AB model. Computations using the MR model are carried out using the material model parameters given in Greensmith's paper (Greensmith, 1963). The elastic constants for the four rubbers used in his experiments are reported in Table 2 of Greensmith's paper. In our simulations, we selected two of these rubbers (vulcanizates A and D in Greensmith's paper). These two rubbers have the largest difference in shear modulus and strain hardening behavior (reflected by c_1/c_2). Since both rubbers obey MR model, we denote them by MR1 and MR2 respectively. Specifically, the constants are: MR1: $c_1=70\,\mathrm{kPa}$, $c_2=80\,\mathrm{kPa}$ ($c_1/c_2=0.88$, $\mu_1=300\mathrm{kPa}$); and MR2: $c_1=239\,\mathrm{kPa}$, $c_2=112\,\mathrm{kPa}$ ($c_1/c_2=2.13$, $\mu_2=902\mathrm{kPa}$). Note that MR1 exhibits less strain hardening than MR2. The uniaxial tension and pure shear behavior of all constitutive models is plotted in Figure 2.

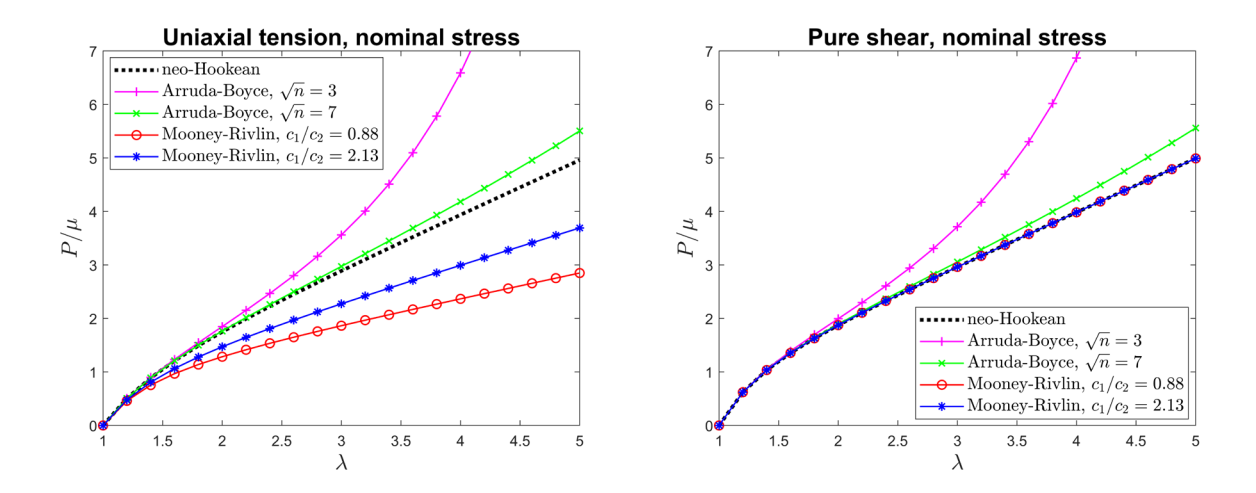


Figure 2: Uniaxial tension (a, left) and pure shear (b, right) behavior of all constitutive models in this work. Nominal stress P in the tension direction normalized by small strain shear modulus μ is plotted versus stretch ratio λ . Notice that in pure shear state, the curves of NH and MR coincide.

3. Finite Element Analysis (FEA)

For each material model, calculations are conducted on two aspect ratios: 10/3 and 5. These values represent the range of aspect ratios used in recent experiments. FEA is carried out using the software ABAQUS. As shown in Figure 3, 6-node, and 8-node quadratic plane stress elements (CPS6, CPS8) are used. The total number of elements is around 4000, and the smallest mesh size near the crack tip is approximately $5 \times 10^{-5} h$. The *J* integral is evaluated using the built-in function in ABAQUS. Several cases with more elements (~ 50000) are tested, and relative differences of values of the J-integral are smaller than 0.1%. More details about the simulation can be found in SI.

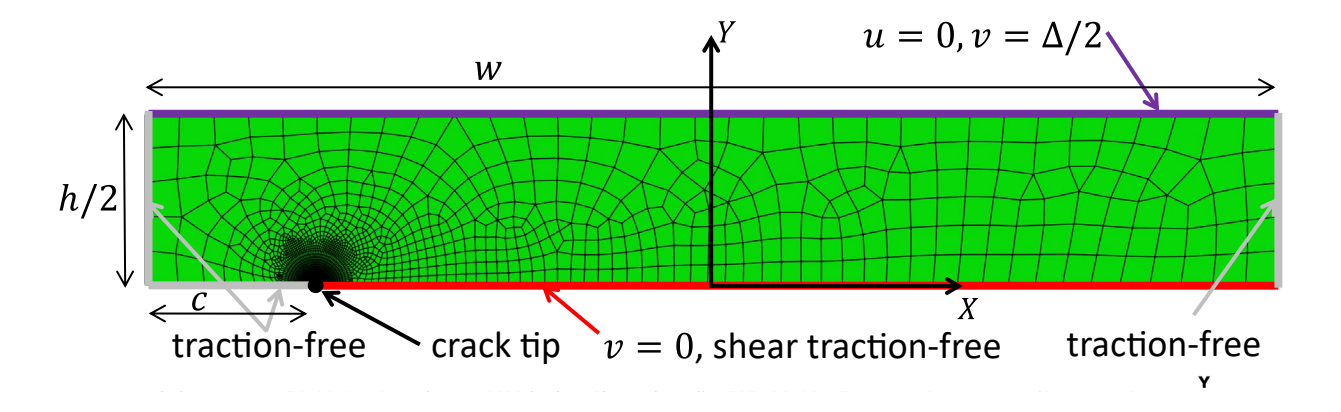


Figure 3: Typical mesh and elements used in FEA. Boundary conditions are indicated, u and v are horizontal and vertical displacement respectively. Only the upper half of specimen is meshed due to symmetry.

Results:

Figure 4 shows the normalized energy release rate \mathcal{J} for NH at four different applied stretch ratios λ . The dash and solid lines represent results for two aspect ratios, w/h = 10/3, 5 respectively. The J integral for short cracks with $c/h \le 0.5$ is practically independent of w/h and yields results consistent with Eq. (4), with α ; 3.7. For w/h = 5, J is within 10% of J_{∞} for $0.1 \le c/w \le 0.9$, or $0.5 \le c/h \le 4.5$, and for different applied stretches. *Interestingly, as the applied stretch increases, J remains closer to J_{\infty} for long cracks, i.e., c/h > 1.* For both aspect ratios, boundary effect becomes significant as the crack approaches the right boundary, resulting in large deviation of J from J_{∞} . As expected, for w/h = 10/3, the edge effect occurs slightly earlier. Specifically, J will be overestimated by 10% at c = 0.85w if we take it to be hW_{∞} , while for w/h = 5, this occurs at c = 0.9w.

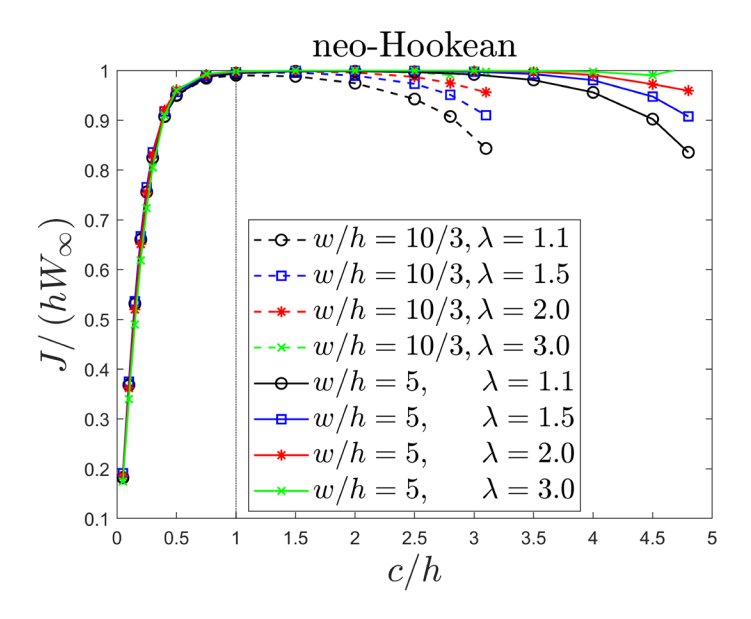


Figure 4: Normalized energy release rate \overline{J} versus c/h for two aspect ratios, w/h = 10/3, 5. Results are plotted for four different applied stretch ratios λ .

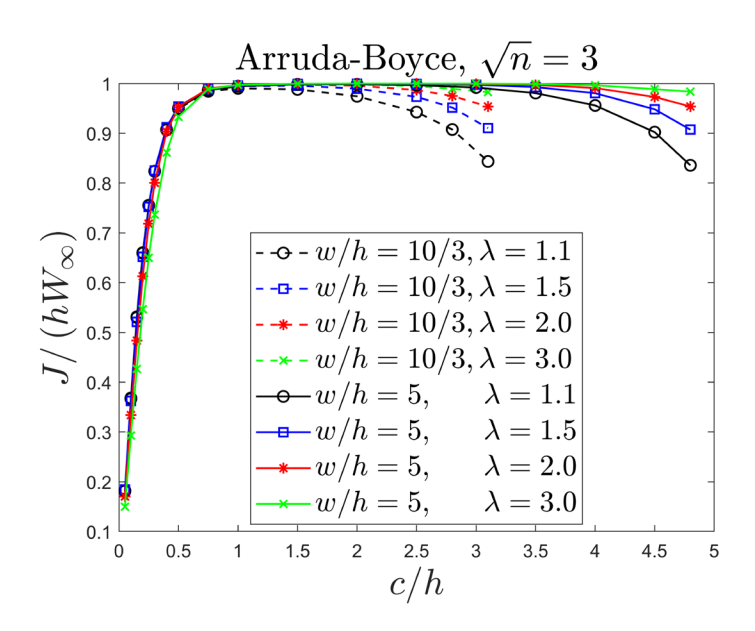


Figure 5: Normalized energy release rate \overline{J} versus c/h for two specimen geometries. Material model is AB with $\sqrt{n} = 3$. Results are for four different applied stretch ratios λ .

Figure 5 plots \overline{J} versus c/h for the AB model with $\sqrt{n}=3$. For the case of $\sqrt{n}=7$, we observed minimal differences in the outcomes. Therefore, the corresponding plot is provided in the Supporting Information (SI). Despite the severe strain hardening characteristics of the AB model, the dependence of the *normalized* energy release on the normalized crack length bears a striking resemblance to that of the NH model. This result supports our scaling analysis, Eq. 3. Similar to NH materials, an increase in the applied stretch ratio prolongs the occurrence of boundary effects, leading to a wider range of crack lengths where $J \approx J_{\infty}$.

Results for MR1 and MR2 are shown in Figure 6a and 6b respectively. While the short crack behavior is practically identical to those of NH and AB, the long crack behavior is different as the edge effect occurs at shorter crack lengths for both aspect ratios. Indeed, even for w/h = 5, deviation of J from its steady value $J_{\infty} = hW_{\infty}$ occurs at shorter crack lengths than NH or AB solids. For example, for w/h = 5, $\lambda = 2$, $J = 0.90J_{\infty}$ at c = 0.7w or 3.5h, whereas for the same stretch ratio, $J = 0.95J_{\infty}$ at c = 0.95w or 4.75h for the AB model with $\sqrt{n} = 3$. For the MR1 specimen with w/h = 10/3, $\lambda = 2$, J never reaches $J = 0.95J_{\infty}$ at any crack length. These deviations are addressed in the discussion.

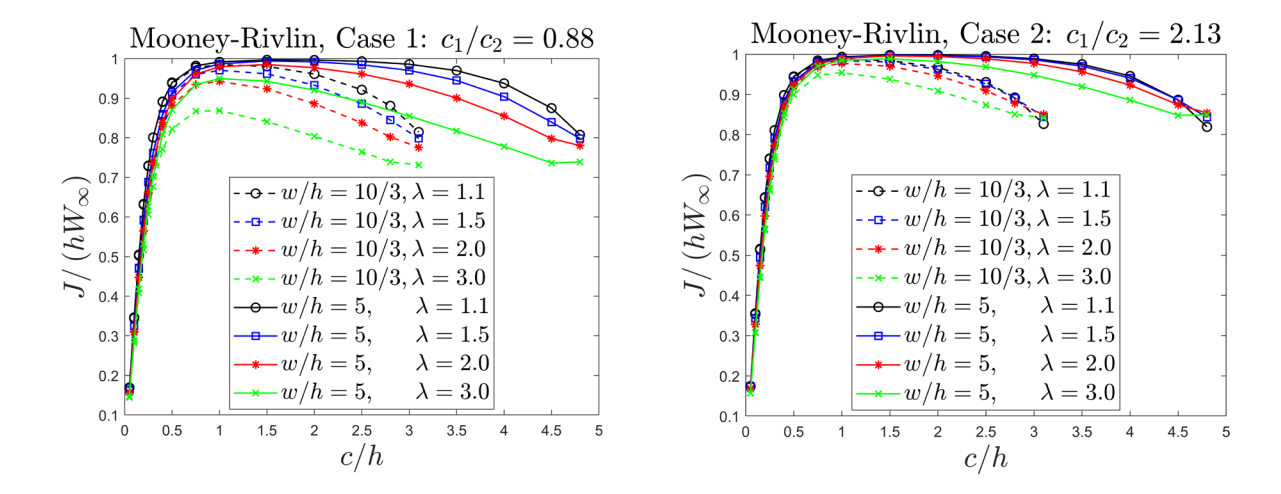


Figure 6: Normalized energy release rate \mathcal{J} versus c/h for two specimen geometries. Results are for four different applied stretch ratios λ . Material model is (a, left) MR1, $c_1/c_2=0.88$, (b, right) MR2: $c_1/c_2=2.13$.

If we disregard the situation where the crack approaches the right boundary, we can obtain a simple and accurate expression for the energy release rate. This expression is obtained by noting that $J \to J_{\infty}$ for long cracks, whereas J must be proportional to $W_{\infty}c$ for short cracks, as demand by Eq. (4). The question is how to determine the proportion constant α in Eq. (4). Our numerical results show that the initial slope α is quite insensitive to the material model, $\alpha \approx 3.7$. Note in our recent work (Wang et al., 2023), we have also found $\alpha = 1.18\pi \approx 3.71$ for a 3-term Yeoh's solid. A function that interpolates from equation (4) to equation (2) is

$$\overline{J} \equiv J / (hW_{\infty}) = \tanh(3.7c/h). \tag{6}$$

Figures 7,8,9 compare the prediction of Eq. (6) with the FEA for stretch ratios of 1.1 and 2. For both stretch ratios, the agreement is excellent for the I_1 -based models like NH and AB. The agreement is less good for the I_1 , I_2 -based model like MR model, especially for smaller aspect ratios and large strains. The results for a larger stretch ratio, $\lambda = 3$, can be found in the SI.

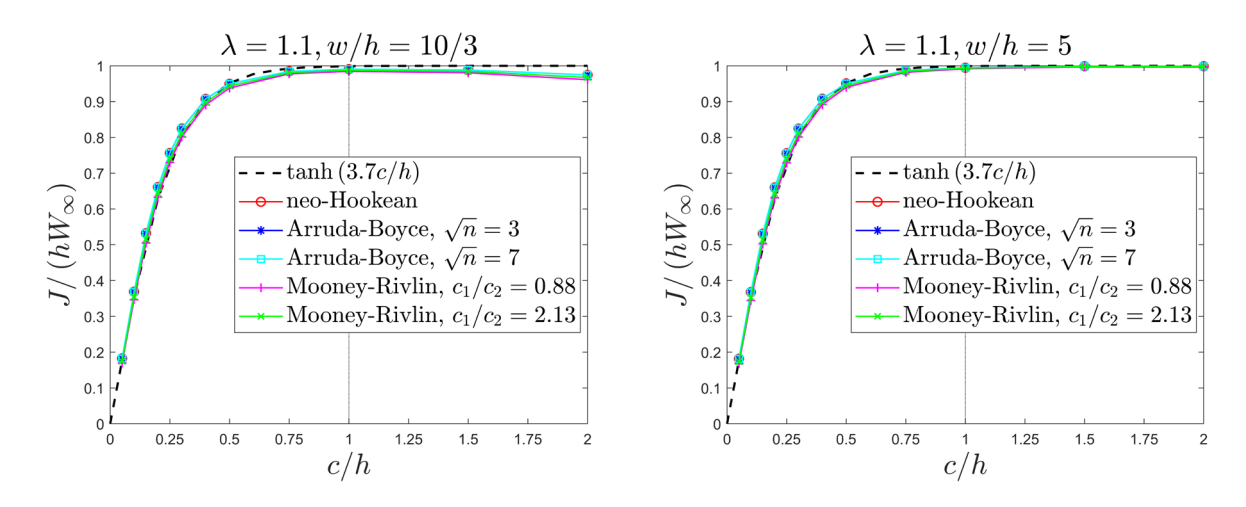


Figure 7: Comparison of Eq. (6) (dashed line) with FEA for different materials. The stretch ratio $\lambda = 1.1$. (a, left) w/h=10/3 (b, right) w/h=5

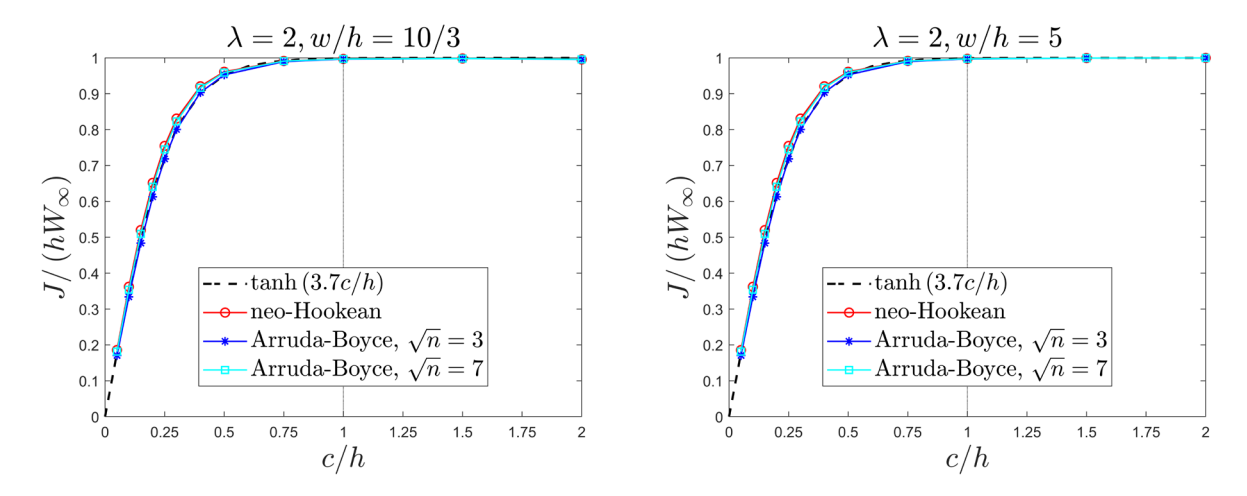


Figure 8: Comparison of Eq. (6) (dashed line) with FEA for materials with strain energy density function that depends only on I_1 . The stretch ratio $\lambda = 2$. (a, left) w/h=10/3 (b, right) w/h=5

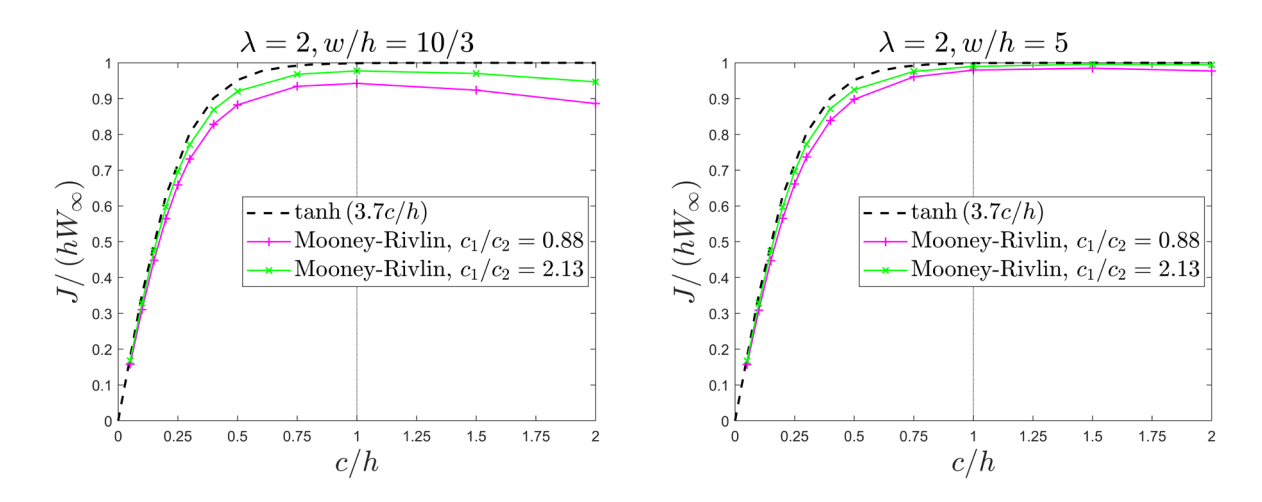


Figure 9: Comparison of (6) (dashed line) with FEA for two Mooney-Rivlin materials. The stretch ratio $\lambda = 2$. (a, left) w/h=10/3 (b, right) w/h=5.

We end this section by tackling a practical question: how to determine W_{∞} ? As mentioned earlier, a commonly employed method involves stretching an *uncracked* PS specimen and graphing the nominal stress against the stretch ratio. Subsequently, the area under the curve is calculated to determine W_{∞} . Yeoh (Yeoh, 2001) demonstrated that the use of this method for a *neo-Hookean* solid can lead to substantial underestimation of the nominal stress, unless very large aspect ratio specimens are employed. This error arises from edge effects and becomes more pronounced as the aspect ratio is decreased. Yeoh's result showed that, for NH solids, this discrepancy decreases as the applied stretch increases. Since neo-Hookean solids lack strain stiffening behavior, it is important to quantify this discrepancy using different hyperelastic models. To achieve this, we used FEA to determine $W(\lambda)$ on uncracked specimens with varying aspect ratios. Our calculations consider the NH, AB and MR models. Figures 10a and 10b display the results for stretch ratios from 1.05 to 5. It is seen that for the NH and AB models the deviation of $W(\lambda)$ from W_{∞} is reduced as strain increases. However, the opposite occurs for the MR models and is more pronounced for MR1, the MR model with the least amount of hardening.

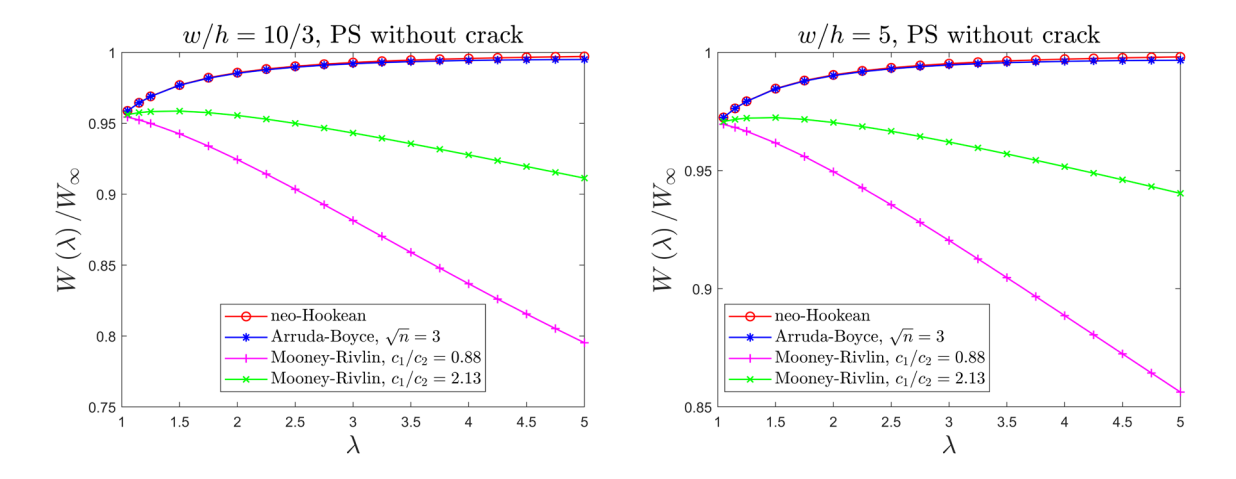


Figure 10: Plot of $W(\lambda)/W_{\infty}$ versus stretch ratio. $W(\lambda)$ is the average strain energy density of uncracked PS specimen calculated using FEM (a, left) w/h=10/3 (b, right) w/h=5.

4. Discussion and Summary

Our analyses show that for typical PS fracture specimens satisfying $10/3 \le w/h \le 5$, J can be well approximated using Eq. (6) for a broad class of hyper-elastic models where the strain energy density depends only on I_1 , provided that $c/h \le 2$. Furthermore, the validity of Eq. (6) extends over a wider range of crack length as the aspect ratio increases. Conversely, smaller aspect ratio specimens exhibit a narrower range of crack lengths where $J = J_{\infty}$, especially for hyper-elastic models like the MR model where energy density depends on both I_1 and I_2 . It is worth noting that J_{∞} is the same for NH and MR materials. This is because $I_1 = I_2$ for an uncracked ideal $(w/h \to \infty)$ PS specimen subjected to uniaxial stretch. For finite-size specimens, c_1/c_2 is an additional factor which affects the convergence of J to J_{∞} , the larger c_1/c_2 corresponds to more strain stiffening. Our numerical result suggests that hyper-elastic models with an energy density that depends on both I_1 and I_2 delays the convergence of J to J_{∞} . As the aspect ratio increases, I_1 and I_2 will become closer to each other at C_3 . Hence there is less reliance on c_1/c_2 in determining the convergence of J to J_{∞} for samples with larger aspect ratios w/h. Our FEM findings support this hypothesis.

Our numerical results suggest that Eq. (4) can be used for short cracks and is largely unaffected by the strain energy density function. However, we do observe slight variations in the initial slope, α , at large strains. Finally, the largest value of the applied stretch ratio we used in our simulations is 3. Our FEA reveals that,

within the range of our study, increasing the stretch ratio expands the range of crack lengths for which $J \approx J_{\infty}$, except for the MR materials.

When utilizing the PS specimen for assessing toughness or crack initiation, our results suggest using a precrack with a length between 0.75h to h. This ensures $J \approx J_{\infty}$, even when dealing with specimens of small aspect ratios. This is consistent with a finding of Kahle et al., (Kahle et al., 2023), where they stated that the deviation of J from J_{∞} is within 10% error for specimens with aspect ratio greater than 2. Here it is important that the crack length of their sample is 20 mm, while the width is w = 60 mm. An aspect ratio of 2 corresponds to h = 30mm, which falls in the regime where $J \approx J_{\infty}$. However, the discrepancy can be quite large if shorter or much longer cracks were used. Therefore, it is important to choose the crack length judiciously for specimens with small aspect ratios. For studying crack growth, it is advisable to opt for the largest possible aspect ratio. This selection helps to maintain a constant value of J in most of the specimens, facilitating the attainment of steady state crack growth.

Based on our numerical results, we observed a decrease in J as the crack approaches the right edge of the specimen. However, we have not specifically investigated the behavior of J as the length of the uncracked ligament approaches zero.

The main results can be summarized as follows:

- For all the hyper-elastic models studied, the energy release rate J for short cracks, i.e., c < h/4 is well approximated by $J \approx 3.7cW_{\infty}$.
- For most of the hyper-elastic models studied, J can be well approximated by Eq. (6) for c ≤ 2h. Also, since the NH and AB model represent two extremes of strain stiffening behavior, we expect Eq. (6) to be valid for hyper-elastic models with energy density that depends only on the strain invariant I₁. One may need to be more careful to use Eq.(6) if the material model is MR and the strain energy density function is highly dependent on the second invariant I₂, especially if the aspect ratio is small and the stretch ratio is high. In this case, the relative error of Eq.(6) can exceed 10%.
- The accuracy and range of validity of Eq. (6) can be improved by increasing the aspect ratio of the PS sample.
- As Figure 10 shows, stretching an uncracked PS sample with an aspect ratio under 5 can underestimate W_{∞} by around 10%. The error lessens with higher stretch ratios and for density functions with sufficient strain stiffening. For MR solids, the trend reverses, notably when $c_2 > c_1$

with higher stretch ratios. Interestingly, this underestimation can be beneficial. For example, in Figure 9(a) with long cracks, the energy release rate J from FEA is below the ideal $J_\infty=hW_\infty$. Using Eqn.(2) or Eqn.(6) with the underestimated W_∞ might yield more accurate results than the ideal W_∞ .

Acknowledgements:

This work is supported by the National Science Foundation, under Grant No. CMMI-1903308.

Reference:

- Arruda, E.M., Boyce, M.C., 1993. A three-dimensional constitutive model for the large stretch behavior of rubber elastic materials. J Mech Phys Solids 41, 389–412. https://doi.org/10.1016/0022-5096(93)90013-6
- Greensmith, H.W., 1963. Rupture of rubber. X. The change in stored energy on making a small cut in a test piece held in simple extension. J Appl Polym Sci 7, 993–1002. https://doi.org/10.1002/app.1963.070070316
- Kahle, E., Ehret, A.E., Mazza, E., 2023. The influence of aspect ratio on the determination of tearing energy in mode I fracture tests. Eng Fract Mech 287. https://doi.org/10.1016/j.engfracmech.2023.109315
- Knowles, J.K., Sternberg, E., 1972. On a class of conservation laws in linearized and finite elastostatics. Arch Ration Mech Anal 44, 187–211. https://doi.org/10.1007/BF00250778
- Mooney, M., 1940. A theory of large elastic deformation. J Appl Phys 11, 582–592. https://doi.org/10.1063/1.1712836
- Pan, Y., Zhou, Y., Suo, Z., Lu, T., 2023. Inelastic zone around crack tip in polyacrylamide hydrogel identified using digital image correlation. Eng Fract Mech 289, 109435. https://doi.org/10.1016/j.engfracmech.2023.109435
- Pidaparti, R.M.V., Yang, T.Y., Soedel, W., 1989. A plane stress finite element method for the prediction of rubber fracture. Int J Fract 39, 255–268. https://doi.org/10.1007/BF00017700
- Qi, Y., Zou, Z., Xiao, J., Long, R., 2019. Mapping the nonlinear crack tip deformation field in soft elastomer with a particle tracking method. J Mech Phys Solids 125, 326–346. https://doi.org/10.1016/j.jmps.2018.12.018
- Rice, J.R., 1968. A path independent integral and the approximate analysis of strain concentration by notches and cracks. Journal of Applied Mechanics, Transactions ASME 35, 379–388. https://doi.org/10.1115/1.3601206
- Rivlin, R.S., 1948a. Large elastic deformations of isotropic materials. IV. Further developments of the general theory. Collected Papers of R.S. Rivlin 241. https://doi.org/10.1007/978-1-4612-2416-7 9
- Rivlin, R.S., 1948b. Large elastic deformations of isotropic materials. I. Fundamental concepts. Philosophical Transactions of the Royal Society of London. Series A, Mathematical and Physical Sciences 240, 459–490. https://doi.org/10.1098/rsta.1948.0002
- Rivlin, R.S., Thomas, A.G., 1953. Rupture of rubber. I. Characteristic energy for tearing. Journal of Polymer Science 10, 291–318. https://doi.org/10.1002/pol.1953.120100303
- Stoček, R., Heinrich, G., Gehde, M., Kipscholl, R., 2013. Analysis of dynamic crack propagation in elastomers by simultaneous tensile- and pure-shear-mode testing, in: Fracture Mechanics

- and Statistical Mechanics of Reinforced Elastomeric Blends. pp. 269–301. https://doi.org/10.1007/978-3-642-37910-9 7
- Tanaka, Y., Kuwabara, R., Na, Y.H., Kurokawa, T., Gong, J.P., Osada, Y., 2005. Determination of fracture energy of high strength double network hydrogels. Journal of Physical Chemistry B 109, 11559–11562. https://doi.org/10.1021/jp0500790
- Treloar, L., 1944. Stress-Strain Data for Vulcanized Rubber under Various Types of Deformation. Rubber Chemistry and Technology 17, 813–825.
- Wang, J., Zhu, B., Hui, C.-Y., Zehnder, A.T., 2023. Delayed fracture caused by time-dependent damage in PDMS. Preprint, Available at SSRN. https://doi.org/10.2139/ssrn.4495461
- Yeoh, O.H., 2001. Analysis of deformation and fracture of "pure shear" rubber testpiece. Plastics, Rubber and Composites Processing and Applications 30, 389–397. https://doi.org/10.1179/146580101101541787
- Zhang, Y., Fukao, K., Matsuda, T., Nakajima, T., Tsunoda, K., Kurokawa, T., Gong, J.P., 2022. Unique crack propagation of double network hydrogels under high stretch. Extreme Mech Lett 51. https://doi.org/10.1016/j.eml.2021.101588
- Zheng, Y., Matsuda, T., Nakajima, T., Cui, W., Zhang, Y., Hui, C.Y., Kurokawa, T., Gong, J.P., 2021. How chain dynamics affects crack initiation in double-network gels. Proc Natl Acad Sci U S A 118. https://doi.org/10.1073/pnas.2111880118